Characterization of Fluorescence Collection Optics Integrated with a Microfabricated Surface Electrode Ion Trap

Craig R. Clark,[1] Chin-wen Chou,[3] A. R. Ellis,[1] Jeff Hunker,[1] Shanalyn A. Kemme,[1] Peter Maunz,[1] Boyan Tabakov,[1,2] Chris Tigges,[1] and Daniel L. Stick[1,2]

[1]*Sandia National Laboratories, P.O. Box 5800, Albuquerque, New Mexico 87185-1082, USA*
[2]*Center for Quantum Information and Control, University of New Mexico, MSC 07-4220, Albuquerque, New Mexico 87131-0001, USA*
[3]*National Institute of Standards and Technology, 325 Broadway Street, Boulder, Colorado 80305, USA*

(Received 12 December 2013; published 27 March 2014)

We demonstrate and characterize a scalable optical subsystem for detecting ion qubit states in a surface electrode ion trap. An array of lithographically fabricated diffractive lenses located below the plane of the trap images ions at multiple locations, relaying the collected light out of the vacuum chamber through multimode fibers. The lenses are designed with solid angle collection efficiencies of 3.58%; with all losses included, a detection efficiency of 0.388% is measured. We measure a minimal effect of the dielectric optical substrate on the temporal variation of stray electric fields and the motional heating rate of the ion.

DOI: 10.1103/PhysRevApplied.1.024004

In recent years, there have been multiple efforts to maximize the efficiency of fluorescence collection from single ions [1–3]. Higher efficiencies lead to higher detection fidelities, shorter detection times, and increased rates of photon-mediated remote ion entanglement [4,5]. In this paper, we focus on another aspect of fluorescence collection, the ability to scale the optical system to simultaneously image multiple ions. Single optics with large fields of view can image multiple ions but sacrifice collection efficiency and are not arbitrarily scalable. Multiple optics each imaging separate locations are scalable if their individual lateral dimensions are comparable to the size of a single trapping well (the exact requirement depends on the specific architecture). In the case of microfabricated surface traps [6], this scalability requires the lateral dimensions of single optics to be smaller than $\approx$1 mm. To simultaneously meet this requirement and still retain a high numerical aperture (NA), the lens must be commensurately close to the ion ($<$ 1 mm). This proximity is generally undesirable due to the physical constraints imposed on the trap electrodes, the reduction of vertical optical access, and issues due to stray charge buildup [7]. Here we describe a system combining ion traps and scalable microfabricated lenses, measure their collection performance, and show that proximity has a manageable impact by measuring the stray electric fields and motional heating rates at different positions in the trap.

Most experiments use multielement refractive lenses outside of the vacuum chamber for imaging ions. These lenses are normally 10–30 mm away from the ion, subtending only a small fraction of the 4π solid angle (SA). Some recent experimental setups explored moving the optic inside the vacuum chamber, including a custom in-vacuum lens (4% SA subtended) [1], a spherical mirror surrounding a trap (10% SA subtended, 0.43% end-to-end detection efficiency) [2], and a microfabricated Fresnel optic with a 5-mm diameter and 3-mm working distance (12% SA subtended, 4.2% effective collection efficiency) [3]. Each of these methods maximizes light collection for single ions in macroscale traps. Other recent experiments focused on demonstrating the size scalability of the collection optics, such as a fiber integrated with a surface electrode trap (2.1% SA subtended) [8] and a micromirror fabricated as part of a surface trap (collection enhancement factor of 1.9 over the free space imaging system) [9]. Here we demonstrate a fiber-coupled array of microfabricated diffractive optic elements (DOEs) with lenses that are slightly smaller than the trapping well size (165-μm focal distance to the ion, 250-μm periodicity), a proof-of-principle experiment combining scalable light collection with integrated microlenses.

The surface electrode ion trap (Fig. 1) used here is operated with a 250-V peak amplitude rf signal at a frequency of 35 MHz. Loading $^{40}Ca^{+}$ is achieved by using a natural calcium source which delivered atoms through the back side of the trap (to prevent the electrodes from being coated) along with lasers for photoionization. After compensation, the resulting secular frequencies of the ion are [1.1, 5.4, 6.2] MHz. More details on the trap fabrication, characterization, and operation can be found in Ref. [10]. The mechanical integration of the collection optic with a surface ion trap is described in detail in Ref. [11].

The array of five lenses is located 165 μm below the ion, with each 140-μm square lens separated by a 110-μm gold ground plane from its neighboring lens, as shown in Fig. 1(a). Each lens is aligned to a multimode fiber with a ceramic ferrule, fixing the lens array's optical axis to the optical axis of the fiber [Fig. 1(b)]. The fiber is connected to a UHV feedthrough for delivering the coupled light outside of the chamber.

UV light in proximity to exposed dielectric surfaces can lead to charge buildup, which is dissipated slowly relative

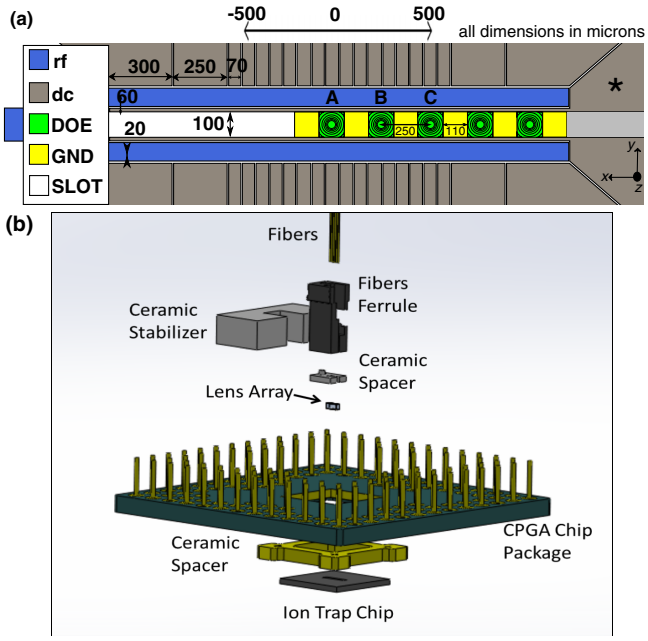

FIG. 1. (a) Plan view of the trap and optics with all dimensions shown in microns [10]. Green squares are the DOEs, gold squares are the gold ground planes between each DOE, and the white region is a slot in the trap for loading ions from the back. The electrode labeled with an * is used to shift the ion in the y direction. (b) Assembly drawing (exploded view) of the optics integrated with the trap chip [11].

to the experiment time. Oxides or contaminants on the trap electrodes can also become charged and generate electric fields at the ion, leading to excess micromotion, which negatively impacts Doppler cooling, light collection, and the motional heating rate of the ion [12–14]. Although the ion is in a direct line of sight with the DOEs, it is significantly shielded by the surrounding electrodes and the grounded gold coating in the space between each DOE, as shown in Fig. 1. Considering this interplay between the different system components, we characterize three properties of the combined trap-optic system: the difference in stray electric fields above and away from the exposed dielectric of the DOE, the motional heating rate difference above and away from the DOE, and the light collection properties of the DOE.

Excess micromotion occurs when the ion is not positioned at the rf null, due to out-of-phase rf signals on different electrodes, an imperfect static trapping solution, or a stray electric field. The first issue can be practically eliminated by capacitively shunting the static control electrodes [10], while the latter two can be eliminated with a static offset applied to the electrodes, provided the stray field does not change on a fast time scale [15]. The stray electric fields are eliminated at multiple locations by employing an adaptive algorithm with iterative measurements of the micromotion along the two transverse axes [15–17]. Combining these techniques allows us to compensate stray fields down to several V/m. After this procedure, the applied voltage solution is compared to boundary element simulations of the trap to estimate the stray field in both the y and z directions.

Figure 2 shows measured stray fields in the y and z directions (radial to the rf confining potential) using an automated compensation procedure, compared at locations away from and above the DOEs. Stray field measurements are taken at a coarse spacing of 77 μm over a total range of ± 500 μm from the center of the x axis of the trap, along with higher-resolution measurements at a 5-μm spacing between optics B and C (Fig. 1).

Figure 2(a) shows a steady increase in the applied field needed to position the ion at the rf null in both the y and z directions, corresponding to the ion's position relative to the DOEs. This increase is primarily due to a modification of the trapping potential by the DOE assembly, as compared to above the open slot at -300 μm. When measured above the slot, the stray field E_z is the same order of

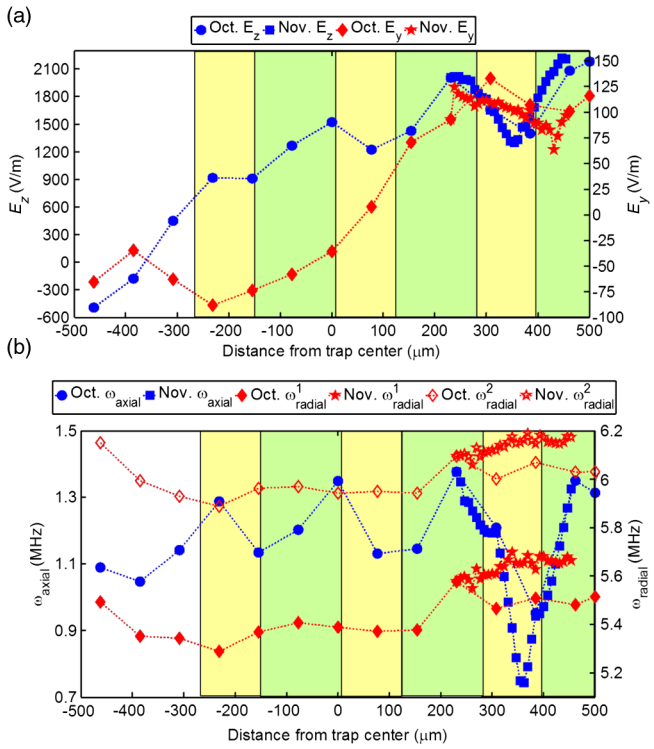

FIG. 2. (a) Stray field measurements of E_z (blue) and E_y (red). The measurement error is 13 V/m in E_z and 3 V/m in E_y. (b) Secular frequency data taken along the z axis of the trap after performing the compensation procedure. (blue) Axial frequency measurements have errors below 1 kHz, and (red) radial frequency measurements have errors less than 10 kHz. Coarse data are taken at 77-μm steps (blue circles and red diamonds); higher-resolution data (blue squares and red stars) are taken a month later between the center of two DOEs at a step size of 5 μm. The background color of the figure corresponds to the different regions of the trap: (white) the loading slot, (gold) ground plane, and (green) DOE. All lines are to guide the eye.

magnitude as E_y, but, as the ion moves above the DOE assembly, E_z dramatically increases. At positions 0, 250, and 500 μm, there are local maxima in E_z of 1500, 2000, and 2200 V/m, which correspond to trapping positions directly above the center of optics A, B, and C, respectively. The local maximum at the position -220 μm corresponds to the edge of the optics mount where the gold ground plane was accidently chipped off during assembly, exposing the dielectric. The local minimum in E_z of 1300 V/m at 350 μm corresponds to storing the ion directly above the gold-coated ground plane between B and C. The secular frequencies show a similar trend due to the stray field. The axial frequency has a local maximum and local minimum corresponding to positions above the DOE and ground plane, respectively. Figure 2(b) also shows the radial frequencies at each location; their fractional change is less significant than that of the axial frequencies and does not exhibit the same spatial modulation. The increase in radial frequency shown on the high-resolution data is ascribed to changes in the helical resonator over the month in which data were taken.

To determine the impact of the DOEs on the temporal stability of the stray electric field, the automated compensation procedure is continuously performed over several hours at locations away from (-385 μm) and above DOE-C (500 μm). Excluding the 15 min following loading, E_y and E_z change less than 2.5 V/m over the following 5 h (below the measurement resolution), while the secular frequencies change less than 1 and 10 kHz in the axial and radial directions, respectively. The loading process results in additional stray fields of $\Delta E_z \approx \pm 25$ V/m and $\Delta E_y \approx \pm 15$ V/m at both locations. Over 5 h, the axial and radial frequencies change less than 2 and 50 kHz, respectively, including the effects of loading. This result would be compatible with high-fidelity two-qubit gates using axial modes of motion ($\delta f/f < 0.2\%$). The greater variability in the radial frequency is ascribed to drift in the resonance frequency of the rf resonator.

A well-known issue with ion traps is the motional heating due to electric field fluctuations on the electrodes [12]. This issue is particularly problematic in traps that confine ions close to trap electrodes (80 μm in the current work). The experiments described here employ the Doppler recooling technique [18] to measure and compare heating rates in the slotted region of the trap and above DOE-C. One set of measurements is taken by using National Instruments voltage sources and yields similar rates above the slot and optic (32 and 42 quanta/ms, respectively). A measurement with a battery voltage supply in the slotted region yields a heating rate of 11 quanta/ms (this method does not allow shuttling an ion to other locations). While these measurements show that the heating rate is comparable near the optic, it should be noted that the overall heating rate of the trap must be reduced to be compatible with high-fidelity two-qubit gates.

The detection efficiency (DE) of each optical system is determined by using a single-photon counting technique [1,2] in which a single photon is emitted with very high probability per experimental sequence. This technique is advantageous, because it does not require calibrating all of the relevant experimental conditions (intensity and detunings of lasers, magnetic field, motional state of ion, etc.) and fitting the calcium atomic spectra to an eight-level optical Bloch equation. The DE values reported in this paper include all system losses, from the solid angle collection to the quantum efficiency of the photomultiplier tube (PMT). The ion is cooled for 2 μs with both lasers, 397 and 866 nm [Fig. 3(a)]. Then it is exposed to a 397-nm laser for 1.5 μs to optically pump to the $D_{3/2}$ state (lifetime = 1 s). A 1.5-μs delay is inserted to ensure the previous laser is fully extinguished. Then the 866-nm laser is turned on to pump to the $P_{1/2}$ state, which decays and generates a single 397-nm photon [Fig. 3(b)]. This sequence is repeated 10^6 times for statistics.

Figure 3(c) is a schematic of both the Standard Imaging (SI) system and the DOE collection setup, along with the transmittance of each optical component. Our standard imaging system includes a grounded mesh to mitigate charge buildup on the reentrant view port. The imaging optic is a UV objective with NA = 0.29 (effective solid angle collection of 1.9%); when combining the view port and optic, the effective solid angle collection is 1.34%. Additional but small losses occur at a UV-coated mirror and filter. Finally, a PMT (Hamamastu H10682-210) is used for photon counting. Considering all these losses, a DE of 0.34% is expected, matching the measured value of $\mathrm{DE_{SI}} = 0.341(6)\%$.

In designing the DOE lens system, the most important metrics are the solid angle collection efficiency and diffraction efficiency. The solid angle collection efficiency of the lens system reported here is calculated to be 3.58%

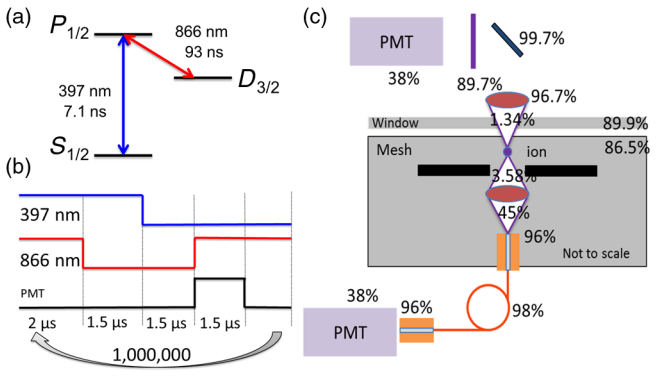

FIG. 3. (a) Ca^+ energy diagram showing the relevant laser transitions. (b) Single-photon generation pulse sequence. (c) Schematic of the standard imaging system and DOE collection system (not to scale). All percentages correspond to the transmittance or reflectivity at 397 nm. The product of each stage results in a total DE of a trapped fluorescing Ca^+ ion.

(this value accounts for the square shape of the lens). Two on-axis lenses are used to image each location in the linear array, as described in Ref. [11]. A standard knife-edge test is used to measure the diffraction efficiency, i.e., the fraction of light transmitted by the lens system into the desired transmitted $\pm$1st order. The range of diffraction efficiencies of 15 fabricated and measured two-lens elements (in series) is 44%–49%, while the integrated lens has an efficiency of 45% and a measured focal distance of 168 μm. The collected light is coupled to a multimode optical fiber (Polymicro's FVP100110125) in which 4% loss is expected at the input and output facets and 2% absorptive loss occurs in the fiber. By using the same PMT as above, a DE_{DOE} of 0.55% is predicted.

Figure 4(a) is an image of the ion after stray electric fields are canceled, along with 397-nm light backilluminating the DOE through the multimode fiber. It shows that the compensated ion is not at the focus of the DOE but is translated in the y direction by almost 20 μm. This conclusion is confirmed after removing the trap from the vacuum chamber and measuring an 18(2)-μm translation, which likely occurred during the bake of the chamber. The height of the focus is *in situ* measured to be at the height of the ion. The backillumination size is larger than the focal spot size of the lens due to the core size of the multimode fiber. For more details on the preinstallation alignment procedure, see Ref. [11].

Additional voltage is applied to the dc control electrodes to shift the ion towards the optic by $\approx$7 μm, as shown in Fig. 4(b). This voltage induced a significant amount of micromotion, but the single-photon counting method is relatively (though not completely) insensitive to micromotion. To quantify the effect, the DE_{SI} is remeasured to be 0.315% corresponding to a drop of 7.6% in the signal compared to the compensated DE_{SI}. Shifting the ion towards the center of the optic increases DE_{DOE} to 0.236 (5)%, compared to 0.023(2)% when compensated. This result is still significantly lower than the theoretical value of 0.51% (which includes the fractional reduction due to micromotion).

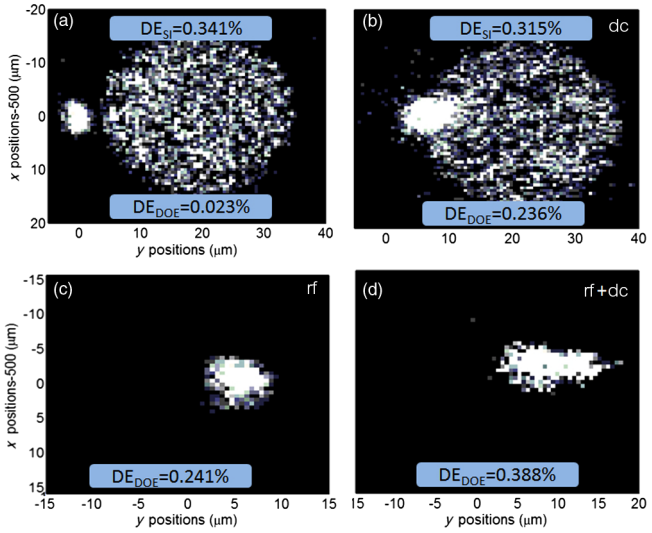

FIG. 4. (a) Image of the compensated ion with corresponding DE_{SI} and DE_{DOE}. (b) Image after applying voltage to the dc electrodes to shift the ion. The large circles in both cases correspond to 397-nm light backilluminating the optic through the fiber. (c) Image after applying rf voltage to the center dc electrode indicated by the star in Fig. 1. (d) Ion after applying both an rf shift and a dc shift of the ion. The smearing of the ion is due to the micromotion.

It is possible to improve DE_{DOE} further by applying an additional rf voltage to one of the center dc electrodes (indicated in Fig. 1 with an *). By reducing the rf amplitude ($V_{rf} = 80$ V) and applying a phase-locked signal to a center electrode, the rf null shifts toward the center of the DOE. Figure 4(c) shows the shift while applying $10V_{rf}$ of phase-locked rf, resulting in an ion displacement of 8 μm and a DE_{DOE} of 0.241(5)%. Figure 4(d) shows the ion displaced by 10–12 μm when both rf and dc fields are used. In this case, $DE_{DOE} = 0.388(6)$%, less than the expected DE of 0.51% due to the remaining imperfect overlap of the ion with the DOE focus.

In conclusion, we demonstrate an integrated array of DOEs with a surface electrode ion trap, coupling fluorescence from a trapped Ca^+ ion into a multimode fiber under ultrahigh vacuum conditions and successfully transmitting the light out of the vacuum chamber to a PMT. Stray electric fields are compensated over the optic and remain stable over the course of weeks, and the DOE does not noticeably affect the motional heating rate of the ion. Using a single-photon counting technique, we measured an overall DE for the DOE of 0.388%. These optics could be arrayed in a scalable fashion and would allow for detection times < 200 μs of Ca^+ with infidelities $< 10^{-4}$ [19]. We show in this paper that their presence does not create stray field drifts that would preclude high-fidelity two-qubit gates and that the heating rate is not noticeably worse near the optic.

We acknowledge and thank Robert Boye for many helpful discussions and M. G. Blain, Joel Wendt, Sally Samora, and the entire fabrication team for providing us with the trap and optics. We also thank Greg Brady for the optical design. This work was supported by the Intelligence Advanced Research Projects Activity (IARPA). Sandia National Laboratories is a multiprogram laboratory managed and operated by Sandia Corporation, a wholly owned subsidiary of Lockheed Martin Corporation, for the U.S. Department of Energy's National Nuclear Security Administration under Contract No. DE-AC04-94AL85000.

[1] M. Almendros, J. Huwer, N. Piro, F. Rohde, C. Schuck, M. Hennrich, F. Dubin, and J. Eschner, Bandwidth-tunable single-photon source in an ion-trap quantum network, Phys. Rev. Lett. **103**, 213601 (2009).

[2] G. Shu, N. Kurz, M. R. Dietrich, and B. B. Blinov, Efficient fluorescence collection from trapped ions with an integrated sherical mirror, Phys. Rev. A **81**, 042321 (2010).

[3] Erik W. Streed, Benjamin G. Norton, Andreas Jechow, Till J. Weinhold, and David Kielpinski, Imaging of trapped ions with a microfabricated optic for quantum information processing, Phys. Rev. Lett. **106**, 010502 (2011).

[4] P. Maunz, S. Olmschenk, D. Hayes, D. N. Matsukevich, L-M. Duan, and C. Monroe, Heralded quantum gate between remote quantum memories, Phys. Rev. Lett. **102**, 250502 (2009).

[5] R. Noek, G. Vrijsen, D. Gaultney, E. Mount, T. Kim, P. Maunz, and J. Kim, High speed high fidelity detection of an atomic hyperfine qubit, Opt. Lett. **38**, 4735 (2013).

[6] J. Chiaverini, R. B. Blakestad, J. Britton, J. D. Jost, C. Langer, D. Leibfried, R. Ozeri, and D. J. Wineland, Surface-electrode architecture for ion-trap quantum information processing, Quantum Inf. Comput. **5**, 419 (2005).

[7] M. Harlander, M. Brownnutt, H. Hänsel, and R. Blatt, Trapped-ion proding of light-induced charging effects on dielectrics, New J. Phys. **12**, 093035 (2010).

[8] A. P. VanDevender, Y. Colombe, J. Amini, D. Leibfried, and D. J. Wineland, Efficient fiber optics detection of trapped ion fluorescence, Phys. Rev. Lett. **105**, 023001 (2010).

[9] J. True Merrill, Curtis Volin, David Landgren, Jason M. Amini, Kenneth Wrigth, S. Charles Doret, C-S. Pai, Harley Hayden, Tyler Killian, Daniel Faircloth, Kenneth R. Brown, Alexa W. Harter, and Richart E. Slusher, Demonstration of integrated microscale optics in surface-electrode ion trap, New J. Phys. **13**, 103005 (2011).

[10] D. T. C. Alllcock, T. P. Harty, H. A. Janacek, N. M. Linke, C. J. Ballance, A. M. Steane, D. M. Lucus, R. L. Jarecki, Jr., S. D. Habermehl, M. G. Blain, D. Stick, and D. L. Moehring, Heating rate and electrode charging measurements in a scalable, microfabricated, surface-electrode ion trap, Appl. Phys. B **107**, 913 (2012).

[11] G. R. Brady, A. R. Ellis, D. L. Moehring, D. Stick, C. Highstrete, K. M. Fortier, M. G. Blain, R. A. Haltli, A. A. Cruz-Cabrera, R. D. Briggs, J. R. Wendt, T. R. Carter, S. Samora, and S. A. Kemme, Integration of fluorescence collection optics with a microfabricated surface electrode ion trap, Appl. Phys. B **103**, 801 (2011).

[12] D. A. Hite, Y. Colombe, A. C. Wilson, K. R. Brown, U. Warring, R. Jördens, J. D. Jost, K. S. McKay, D. P. Pappas, D. Leibfried, and D. J. Wineland, 100-fold reduction of electric-field noise in an ion trap cleaned with in situ argon-ion-beam bombardment, Phys. Rev. Lett. **109**, 103001 (2012).

[13] S. Charles Doret, Jason M. Amini, Kenneth Wright, Curtis Volin, Tyler Killian, Arkadas Ozakin, Douglas Denison, Harley Hayden, C.-S. Pai, Richart E. Slusher, and Alexa W. Harter, Controlling trapping potentials and stray electric fields in a microfabricated ion trap through design and compensation, New J. Phys. **14**, 073012 (2012).

[14] A. Safavi-Naini, E. Kim, P. F. Weck, P. Rabl, and H. R. Sadeghpour, Influence of monolayer contamination on electric-field-noise heating in ion traps, Phys. Rev. A **87**, 023421 (2013).

[15] D. J. Berkeland, J. D. Miller, J. C. Bergquist, W. M. Itano, and D. J. Wineland, Minimization of ion micromotion in a paul trap, J. Appl. Phys. **83**, 5025 (1998).

[16] Y. Ibaraki, U. Tanaka, and S. Urabe, Detection of parametric resonance of trapped ions for micromotion compensation, Appl. Phys. B **105**, 219 (2011).

[17] S. Narayanan, N. Daniilidis, S. A. Möller, R. Clark, F. Ziesel, K. Singer, F. Schmidt-Kaler, and H. Häffner, Electric field compensation and sensing with a single ion in a planar trap, J. Appl. Phys. **110**, 114909 (2011).

[18] R. J. Epstein, S. Seidelin, D. Leibfried, J. H. Wesenberg, J. J. Bollinger, J. M. Amini, R. B. Blakestad, J. Britton, J. P. Home, W. M. Itano, J. D. Jost, E. Knill, C. Langer, R. Ozeri, N. Shiga, and D. J. Wineland, Simplified motional heating rate measurements of trapped ions, Phys. Rev. A **76**, 033411 (2007).

[19] A. H. Myerson, D. J. Szwer, S. C. Webster, D. T. C. Allcock, M. J. Curtis, G. Imreh, J. A. Sherman, D. N. Stacey, A. M. Steane, and D. M. Lucas, High-fidelity readout of trapped-ion qubits, Phys. Rev. Lett. **100**, 200502 (2008).